Eur. Phys. J. B **50**, 403–410 (2006)
DOI: 10.1140/epjb/e2006-00154-5

THE EUROPEAN PHYSICAL JOURNAL B

Longitudinal-optical phonon hole-plasmon coupled modes in heavily doped p-type GaSb:Zn epitaxial films

Z.G. Hu[1,a], M.B.M. Rinzan[1], A.G.U. Perera[1,b], Y. Paltiel[2], A. Raizman[2], A. Sher[2], and M. Zhu[3,c]

[1] Department of Physics and Astronomy, Georgia State University, Atlanta, Georgia 30303, USA
[2] Electro-Optics Division, Soreq Nuclear Research Center (NRC), Yavne 81800, Israel
[3] Department of Physics, Shanghai Jiao Tong University, 1954 Hua Shan Road, Shanghai 200030, P.R. China

Received 25 August 2005 / Received in final form 10 January 2006
Published online 5 May 2006 – © EDP Sciences, Società Italiana di Fisica, Springer-Verlag 2006

Abstract. Reflectance measurements from p-type GaSb:Zn epitaxial films with different hole concentrations (10^{17}–10^{18} cm^{-3}) have been investigated over the frequency region of 100–1000 cm^{-1}. A minimum broadening feature corresponding to the hole plasmon was observed in the reflectance spectra. The experimental infrared spectra were well fitted using a Lorentz-Drude dispersion model. The real part ε_1 of the dielectric function decreases with increasing hole concentration. However, the imaginary part ε_2 increases with hole concentration in the far-infrared region. This indicates that the acoustic- and optic-phonons mainly participate in the free carrier absorption processes. The hole mobility obtained from Hall-effect measurements is slightly larger than that derived from optical measurements and the average ratio of mobilities is estimated to be 1.33. Owing to overdamping effects, the upper branch of longitudinal-optical phonon plasmon (LPP) coupled modes was observed. The upper LPP$^+$ frequency increases with hole concentration and it shows a transition from phonon-like to plasmon-like behavior. A theoretical analysis with solutions in the complex frequency plane describes these experimental results.

PACS. 78.20.Ci Optical constants (including refractive index, complex dielectric constant, absorption, reflection and transmission coefficients, emissivity) – 78.30.Fs III-V and II-VI semiconductors – 81.70.Fy Nondestructive testing: optical methods

1 Introduction

Among III–V group semiconductors, gallium antimonide (GaSb) is particularly interesting for optoelectronics device applications [1]. The far-infrared (FIR) optical properties and/or lattice vibrations of GaSb bulk material have been investigated for several decades [2–4]. Recent progress in film growth techniques, such as metalorganic vapor-phase epitaxy (MOVPE) and molecular beam epitaxy (MBE), makes it possible to study the optical properties of GaSb epitaxial films. In order to achieve a high p-type doping, zinc (Zn) is commonly used, in which case the electrical properties have been studied before [5]. However, valuable information for infrared optoelectronic application of p-type GaSb:Zn epilayers are scarce. These properties are significant for the design and development of p-type GaSb-based infrared detectors, which may have better properties than the already successful GaAs-based FIR detectors [6].

One of the main parameters needed for optoelectronic device design is the interaction of free carriers with photons in the low frequency region [7,8]. For FIR or terahertz (THz) detector design, the detailed and accurate knowledge of the dielectric function is necessary to evaluate the total optical absorption of the detectors. In order to improve the performance of $Al_xGa_{1-x}As$/GaAs THz detectors, a detailed study of the dielectric functions for p-type $Al_xGa_{1-x}As$ films was done [9], and followed by the design and realization of high performance detectors [10]. The dielectric function of the GaSb material related to the high-energy critical point transitions has been studied by Adachi [11]. Paskov reported the dielectric function of GaSb with different carrier concentrations [12]. However, these studies were limited to regions near and beyond the optical band-gap energy (about 0.7 eV). Few reports were made on the infrared dielectric functions of $Al_xGa_{1-x}Sb$ and GaSb [13,14]. Nevertheless, very few results were presented on the low frequency dielectric functions of p-type GaSb:Zn epilayers.

[a] *Present address:* Institute of Physical Chemistry, University of Heidelberg, Im Neuenheimer Feld 253, 69120 Heidelberg, Germany
e-mail: Zhigao.Hu@urz.uni-heidelberg.de
[b] e-mail: uperera@gsu.edu
[c] Also at Department of Educational Information and Technology, School of Educational Science, East China Normal University, North Zhongshan Road 3663, Shanghai, 200062, P.R. China.

In polar semiconductors, plasmons of free carriers interact with longitudinal optical (LO) phonons via their macroscopic electric field [15]. The LO-phonon plasmon (LPP) coupled modes, which are interesting for the physical interactions between the lattice vibrations and free carriers, can be directly investigated using infrared reflectance spectra [16,17]. In principle, the LPP coupled modes should form two modes with frequencies quite different from the fundamental modes and suppress the unscreened LO phonon with increasing carrier concentration. The LPP coupled modes for n-type semiconductors have been intensively investigated using both theoretical and experimental approaches [15,18]. Recently, the LPP coupled modes of p-type GaAs epitaxial films with different hole concentrations have been studied using Raman scattering and infrared reflectance spectra [9,19–21]. However, little is known on the LPP coupled modes for other III–V group semiconductor films [22,23]. To our knowledge, there exists no studies on the LPP coupled modes of GaSb. The upper LPP coupled mode has not been observed in Raman scattering for p-type III–V group materials owing to a higher damping constant, higher hole effective mass, and lower hole mobility [20,24]. However, infrared reflectance spectra could be suitable to investigate the LPP coupled modes for p-type III–V group semiconductor films. Although Raman scattering and infrared spectroscopy can be used to estimate the plasma frequency and carrier mobility of semiconductor materials, the main differences between the two methods are potentially different selection rules, and the penetration of the exciting radiation, and thus also the region of the sample in the measurement [21,22].

In this article, the far-infrared optical properties of p-type GaSb:Zn epilayers with different hole concentrations are investigated. A theoretical analysis with a three-phase configuration and Lorentz-Drude dielectric function model is presented to explain the experimental reflectance data. The detailed dependencies of the dielectric function and the LPP coupled modes on the hole concentration will be discussed.

2 Experimental details

GaSb epitaxial films were grown on p-type GaSb substrates at a temperature of 600° C and reactor pressure of 400 torr by metalorganic vapor-phase epitaxy (MOVPE) deposition technique. The epilayers were deposited using a Thomas-Swan vertical reactor. The GaSb films were Zn-doped with diethylzinc as a dopant source and exhibit p-type conductivity. The nominal film thickness is 1.3 μm for all GaSb epilayers. Note that the samples were simultaneously grown on both p- and n-type GaSb substrates. Reliable Hall mobility results at room temperature were obtained as the p-n junction was found to be efficient in electrically isolating the p-type epilayer from the n-type substrate [8].

Infrared reflectance spectra for five GaSb epilayers were measured over the frequency range of 100–1000 cm^{-1} using a nitrogen purged Perkin-Elmer system 2000 Fourier Transform Infrared (FTIR) spectrometer. The spectra were recorded in near-normal incidence (the angle of incidence is about 8°) using a spectral reflectance accessory. The incident light-spot area on the epilayers was about 4 mm in diameter. For the high frequency region of 450–1000 cm^{-1}, a liquid-nitrogen cooled MCT detector and optimized KBr beam splitter were used with a resolution of 4 cm^{-1}. A TGS/POLY detector and 6-μm-thick mylar beam splitter were employed for the measurements in the low frequency region of 100–700 cm^{-1} with a resolution of 2 cm^{-1}. Gold (Au) and aluminum (Al) mirrors, whose absolute reflectances were directly measured, were used as references for the spectra in the high and low frequency regions, respectively. The samples were at room temperature for all measurements and no mathematical smoothing has been performed on the experimental reflectance data.

3 Results and discussion

3.1 Theoretical model

The reflectance of a single film on a substrate can be calculated by Snell′s law considering the film to be isotropic [9,25]. The optical component of each layer is expressed by a 2 × 2 matrix. Suppose "0" refers to vacuum, whose dielectric function is unity, "1" the film, and "2" the substrate, respectively. The resultant matrix M_r is described by the following:

$$M_r = M_{01} M_1 M_{12}. \tag{1}$$

Here, the interface matrix between the jth and $(j+1)$th layers has the form

$$M_{j,j+1} = \frac{1}{2\sqrt{\tilde{\varepsilon}_{j+1}}} \begin{bmatrix} \left(\sqrt{\tilde{\varepsilon}_{j+1}} + \sqrt{\tilde{\varepsilon}_j}\right) & \left(\sqrt{\tilde{\varepsilon}_{j+1}} - \sqrt{\tilde{\varepsilon}_j}\right) \\ \left(\sqrt{\tilde{\varepsilon}_{j+1}} - \sqrt{\tilde{\varepsilon}_j}\right) & \left(\sqrt{\tilde{\varepsilon}_{j+1}} + \sqrt{\tilde{\varepsilon}_j}\right) \end{bmatrix}, \tag{2}$$

and the propagation matrix for the film with thickness d (1.3 μm) is described by

$$M_1 = \begin{bmatrix} \exp(i2\pi\sqrt{\tilde{\varepsilon}}d/\lambda) & 0 \\ 0 & \exp(-i2\pi\sqrt{\tilde{\varepsilon}}d/\lambda) \end{bmatrix}, \tag{3}$$

where λ is the incident wavelength. Thus, the reflectance R can be readily obtained from

$$R = \left| \frac{M_{r1,0}}{M_{r1,1}} \right|^2. \tag{4}$$

The multiple reflections from the substrate are not considered in equation (4) because there are strong phonon and free carrier absorptions for p-type GaSb substrate in the region of interest. That is to say, the penetration depth of the incident infrared light in the GaSb substrate is so short that the reflection from the rough backside is negligible.

For polar semiconductor materials, the dielectric response can be described by the harmonic Lorentz oscillator model. The contribution from free carriers to the

dielectric function for doped semiconductors is commonly written in the classical Drude model. The dielectric function ($\tilde{\varepsilon} = \varepsilon_1 + i\varepsilon_2$) of the GaSb:Zn epitaxial films can be written as the Lorentz-Drude model:

$$\tilde{\varepsilon} = \varepsilon_\infty + \frac{S\omega_{TO}^2}{\omega_{TO}^2 - \omega^2 - i\omega\Gamma} - \frac{\varepsilon_\infty \omega_p^2}{\omega^2 + i\omega\gamma}. \quad (5)$$

Here, ε_∞, ω_{TO}, S, Γ, ω_p and γ represent the high-frequency dielectric constant, transverse-optical (TO) phonon frequency, the oscillator strength, the broadening value of TO phonon, the plasma frequency and the phenomenological damping constant, respectively. The plasma frequency and the mobility μ of free carriers are given by the following two relations: $\omega_p^2 = pq^2/\varepsilon_o\varepsilon_\infty m^*$ and $\mu = q/2\pi c m^* \gamma$, here m^* is the average hole effective mass, p the carrier concentration, q the electron charge, and ε_o the vacuum permittivity. It should be stated that there are other dielectric function models such as hydrodynamic and Lindhard-Mermin models, which consider the spatial dispersion, the intraband and interband contributions in the analysis of Raman scattering [22,26–29]. However, a wavevector term is introduced in order to include momentum dependence in the scattering process [27–29]:

$$\omega_p^2 = \frac{pq^2}{\varepsilon_o\varepsilon_\infty m^*} + \frac{3k^2 v_f^2}{5}. \quad (6)$$

Here, $k = 2\nu n$, where ν is the wavevector of the incident light for back scattering configuration in Raman scattering, n is the refractive index of the material, and v_f is the Fermi velocity, which depends on the parabolic or nonparabolic valence bands [28]. The second term of equation (6) is a second-order effect of a plasma quantum, arising from nonlocal effects owing to the noncompressibility of the system, and it does not appear in the above classical treatment of equation (5). Infrared reflectance, which is based on the conservation of energy (Eq. (4)), is not sensitive to the momentum change (i.e., small variations of the wavevector) because the film thickness is very small (1.3 μm) compared to the wavelengths of interest (above 10 μm). In addition, the momentum conservation could be relaxed owing to a stronger absorption from the heavily doped GaSb:Zn epilayers. Generally, Raman scattering with visible laser excitation can result in a diffraction-limited laser spot of less than 1 μm while a typical infrared spectrometry gives an illuminated spot of around 100 μm. Therefore, the contribution from higher order terms could be neglected for infrared reflectance experiments, but in Raman scattering, it becomes a effective factor and is about 10% of the first term of equation (6) [22,28,29]. Correspondingly, it means that the equation (5.2) in reference [22] and equation (2) in reference [27] regress to the first term of equation (6) here. In addition, the classical Drude model is the simplest and widely used in FIR or THz reflectance spectra in order to avoid the strong parameter correlations in the fitting [30,31]. Moreover, it can provide a relatively good approximation within the experimental errors [7,9,21,24,29–32].

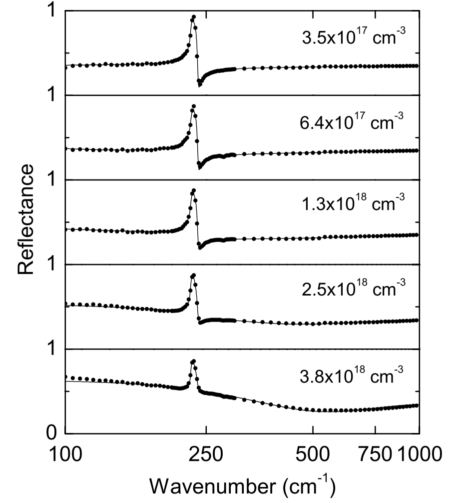

Fig. 1. Experimental reflectance spectra (dotted lines) of the GaSb:Zn epitaxial films with different hole concentrations. Best-fit results are presented with solid lines. To distinguish between the results, the spectra are successively shifted vertically by 1. The logarithmic horizontal scale enlarges the reststrahlen region.

Figure 1 displays the experimental (dotted lines) and theoretical (solid lines) reflectance spectra of the GaSb:Zn epilayers. A good agreement between experimental and calculated spectra was obtained over the entire frequency region. The best fit parameter values together with their errors are listed in Table 1. In all spectra, a clear peak around 227 cm^{-1} is assigned to the TO-phonon mode. A broadening reflectance minimum can be identified for the samples with the two highest hole concentrations. This minimum is a hole-plasmon feature in p-type GaSb:Zn epilayers. The coupling interaction between the free carrier plasmon and LO phonon strongly affects the pattern of the phonon band while its position stays constant. Moreover, the reflectance in the reststrahlen band decreases with hole concentration, indicating that the coupling increases and separates the unscreened LO phonon and plasma frequencies into modes with different energies [9,21,24].

3.2 Dependence of the dielectric function on the free hole concentration

From Table 1, the high-frequency dielectric constant of GaSb epilayers varies approximately from 14.8 to 15.6. These are slightly higher than the reported value of 14.5 [14]. Note that the parameter ε_∞ accounts for the so-called high-frequency limit. Therefore, the dielectric function model should be extrapolated to shorter wavelengths than those studied here. However, it is nearly impossible that the Lorentz-Drude model expressing the phonon and free carrier characteristics can explain the complicated behavior of many high-energy transitions (above the band-gap energy) in semiconductor materials. The high-frequency dielectric constants are determined with a higher precision for the GaSb:Zn epilayers with the

Table 1. Lorentz-Drude parameter values of p-type GaSb:Zn epitaxial films deduced from the best fit to the infrared reflectance spectra in Figure 1. The 90% confidence limits are given in brackets. Hole concentrations p are determined from Hall-effect measurements. The longitudinal-optical (LO) phonon frequencies are calculated from the relationship $\omega_{LO}^2 = (S/\varepsilon_\infty + 1)\omega_{TO}^2$. The hole mobilities of optical (μ_{IR}) and Hall-effect (μ_{Hall}) measurements are compared.

Samples	p (10^{17} cm^{-3})	ε_∞	S	ω_{TO} (cm^{-1})	Γ (cm^{-1})	ω_{LO} (cm^{-1})	ω_p (cm^{-1})	γ (cm^{-1})	μ_{IR} [cm^2/(Vs)]	μ_{Hall} [cm^2/(Vs)]	μ_{Hall}/μ_{IR}
A	3.5	15.1	1.36	226.5	1.7	236.5	90.2	116.0	313	410	1.31
		(0.1)	(0.02)	(0.1)	(0.1)		(2.8)	(11.0)			
B	6.4	14.8	1.28	226.7	2.8	236.3	105.9	48.7	552	390	0.71
		(0.1)	(0.02)	(0.1)	(0.1)		(2.5)	(4.5)			
C	13	14.9	1.30	226.7	2.4	236.4	137.7	114.1	199	280	1.41
		(0.1)	(0.02)	(0.1)	(0.1)		(1.3)	(5.1)			
D	25	15.5	1.28	226.7	1.7	235.9	222.0	193.6	164	200	1.22
		(0.1)	(0.03)	(0.1)	(0.2)		(1.5)	(5.4)			
E	38	15.6	1.30	226.9	1.9	236.2	316.6	226.2	190	260	1.37
		(0.1)	(0.06)	(0.2)	(0.3)		(2.0)	(5.8)			

three lowest hole concentrations because the contributions from high-energy electronic transitions can be neglected. A wider spectral region is required for the samples D and E in order to increase the determination precision. Nevertheless, the values of 15.5 and 15.6 remain reasonable taking into account the experimental uncertainties. The broadening of the TO phonon is about 2.0 cm^{-1} for all the samples indicating that the phonon pattern are sharp for the GaSb films as shown in Figure 1. The broadening is higher than the value of GaSb bulk crystal (0.95 cm^{-1}) [14]. This may be due to the disorder and stress effects in the epilayers. The TO- and LO-phonon frequencies are 227 cm^{-1} and 236 cm^{-1}, respectively, and remain constant with different hole concentrations. These results indicate that the hole concentration has no influence on the phonon modes of the GaSb:Zn epilayers in the present work.

Using equation (5) with the parameter values from Table 1, the dielectric functions of the epilayers are calculated. Figure 2 shows the dielectric function of the GaSb film with hole concentration of 3.8×10^{18} cm^{-3}. This hole concentration is a good representative of all other measurements over the entire measurement range. At the wavelength of 10 μm, the estimated refractive index is about 3.8, which is close to the theoretical value of 3.9 in the transparent region [12]. It is known that the hole concentration mainly affects the far-infrared responses of III–V semiconductor films [8,9]. From the inset in Figure 2, the real part ε_1 decreases with increasing hole concentration except for sample B, whose hole damping constant is minimum (Tab. 1). The imaginary part ε_2 increases with hole concentration indicating that the far-infrared absorption coefficient increases [8]. For the GaSb:Zn films with higher hole concentrations, ε_2 increases quickly with decreasing optical frequency. This is typical of free carrier absorption in semiconductor materials [33]. In this case, the third term (Drude model) in equation (5) plays an important role in the dielectric response of the films. Correspondingly, the extinction coefficient is larger than the refractive index, which results in negative values of ε_1 in the far-infrared region.

The free carrier absorption (FCA) is an important intraband transition process of semiconductors, which corresponds to the transition from the low-energy to high-energy sub-states in the same band (the valence bands for p-type GaSb:Zn films). It is an indirect transition process and normally requires the participation of other quasi-particles (such as phonons and ionized dopants) in order to conserve the momentum [34,35]. The free carrier absorption coefficient increases with the wavelength above the phonon frequency and can be experimentally described by the relationship $\alpha(\lambda) = K\lambda^m$ [36]. Here, the proportional coefficient K depending on doping concentration and the exponential factor m indicates the species of quasi-particles in the intraband transition, which varies from 1.5 to 3.5 owing to different quasi-particle participation. For III–V group semiconductors, the exponential factor of 1.5 ∼ 2.0, 2.5, and 3.0 ∼ 3.5 refer to the participation from acoustics-phonons, optic-phonons, and ionized dopants, respectively [34,36]. In general, it is noted that all three species can contribute to the carrier absorption process. Therefore, the exponential expression gives

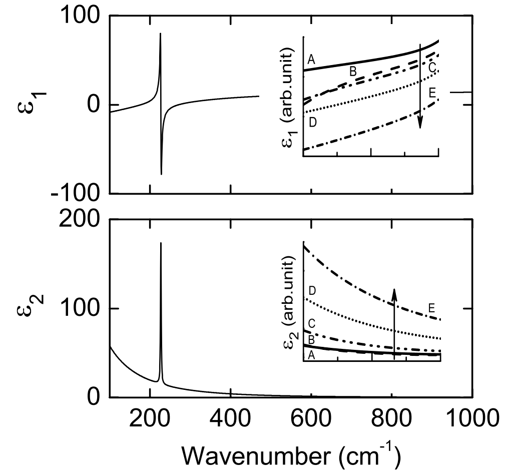

Fig. 2. The infrared dielectric function for a GaSb:Zn film with hole concentration 3.8×10^{18} cm^{-3}. The dielectric functions of the GaSb:Zn epilayers of different hole concentrations in the wavenumber region of 100–200 cm^{-1} (50–100 μm) are given in the inset. The arrows indicate increasing hole concentration.

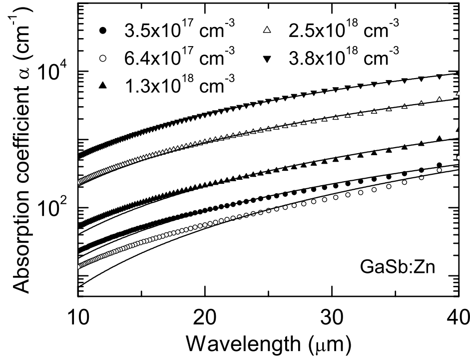

Fig. 3. The infrared absorption coefficients (dotted lines) of GaSb:Zn epilayers in the wavelength region of 10–40 μm (250–1000 cm^{-1}). The calculated dependencies of the absorption coefficient on the wavelength are plotted for comparison (solid lines). The detailed discussions can be found in Section 3.2.

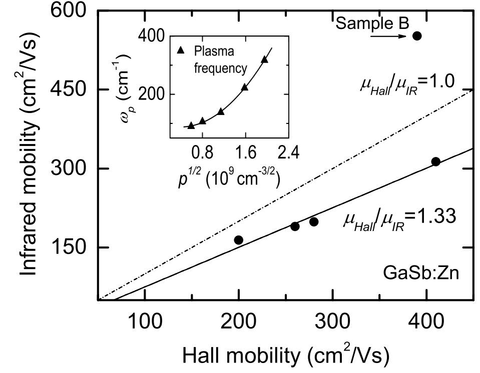

Fig. 4. The Hall mobility versus the infrared mobility of the GaSb:Zn epilayers. The inset shows the dependence of the plasma frequency of the GaSb:Zn epitaxial films on the value of $p^{1/2}$. The sublinear relationship (solid line in the inset) indicates that the hole effective mass strongly depends on the carrier concentration.

an approximate evaluation from all three contributions and correspondingly decreases the fitting uncertainty. Figure 3 shows the infrared absorption coefficients of GaSb:Zn epilayers beyond the phonon frequency and the fitted values using the above relationship, respectively. The calculated proportional coefficient K increases from 0.01 to 5.7 and important exponential factor m varies between 2.0 and 2.9, which agree with those of GaSb bulk crystals from reference [36]. The fitting quality increases with the hole concentration, which indicates that the effects from the free carriers become more prominent in infrared absorption process. It should be emphasized that the intervalence band absorption by holes is not taken into account in the analysis. However, for p-type GaSb epilayers, the FCA by holes can be expected to contribute significantly to the absorption for the longer wavelengths, which are far from the fundamental band-gap in the present work (above 10 μm). Although it is difficult to distinguish the independent participation from the three species, it can be concluded that the acoustic- and optic-phonon contributions are the main absorption mechanisms in the FCA processes of the GaSb:Zn epilayers with the hole concentrations of 10^{17}–10^{18} cm^{-3}, based on the fitted m values.

3.3 Comparison on free hole mobility between IR and Hall-effect measurements

Heavily doped semiconductor films normally have large inhomogeneities, which can affect the electrical transport properties [17]. Electrical characterization (such as Hall-effect measurements) require the forming of electrical contacts, which restricts the use of the sample. Infrared reflectance spectroscopy is a non-intrusive technique, which is an attractive and powerful tool for physical characterization of films. Furthermore, infrared spectra can be used to directly estimate the transport properties of some doped semiconductors [32,35,37]. As shown in Table 1, the plasma frequency increases with the hole concentration. However, the damping constant shows a more complex behavior. The comparison between Hall mobility (μ_{Hall}) and IR mobility (μ_{IR}) is presented in Table 1. Figure 4 shows the IR mobility from the reflectance measurements together with the Hall mobility of the GaSb:Zn epilayers. In most cases, the Hall mobility appears to be slightly larger than the IR mobility except for sample B, whose mobility is maximum owing to a minimum damping constant (48.7 $\pm$ 4.5 cm^{-1}). In order to check whether the hole concentration of sample B presents a true singularity, more optical measurements will be necessary. A detailed study of this phenomenon is currently under way with new samples using Raman scattering. The average value of μ_{Hall}/μ_{IR} ratio is 1.33 except for sample B (a minimum value of 0.71) and the calculated value $\mu_{Hall}/\mu_{IR} = 1.0$ are also shown in Figure 4. The discrepancy between Hall-effect and optical reflectance was previously investigated for p-type GaAs films and an average μ_{Hall}/μ_{IR} ratio was reported between 1.5 and 3.7 [15,24]. This indicates that the scattering time at low frequencies is significantly smaller than that in DC fields. The Hall factor is routinely ignored in Hall-effect measurements of the mobility and carrier concentration. This is equivalent to assuming that the Hall factor is equal to unity. However, this assumption results in some errors and in theory the value can be expected to be larger than unity as shown in Figure 4. On the other hand, the Drude part of equation (5) is only an approximation while a more correct approach should take frequency changes into account. It can be written as follow [24]

$$\varepsilon_{Drude}(\omega) = \varepsilon_\infty \left\langle \frac{\omega_p^2}{\omega^2 + i\omega\gamma(\omega)} \right\rangle. \tag{7}$$

Here, the symbol "$\langle\ \rangle$" indicates the average value. The simplified Drude form, which accounts only for the average value of the damping constant, could be the major cause for the discrepancy between electrical and optical mobilities [24]. The more rigorous theory (Eq. (7)) would take into account the average carrier-energy distribution

at each light frequency. Nevertheless, the approach becomes very complicated in fitting infrared reflectance spectra and the present simple approximation gives reasonable results indicating that the ratio μ_{Hall}/μ_{IR} is slightly larger than unity [38].

The inset of Figure 4 demonstrates a changing trend in the plasma frequency with the square root of the hole concentration. The sub-linear relationship shows a strong hole effective mass dependence on the carrier concentration. The hole effective mass from the optical measurements varies from 0.22 to $0.41m_0$, where m_0 is the free electron mass. Heller et al. reported a value of $(0.28 \pm 0.13)m_0$ for GaSb bulk with a hole concentration of 1.2×10^{17} cm^{-3} at low temperature [39]. Owing to the complexity of the holes in *p*-type semiconductors, the theoretical calculation will be difficult considering the splitting of the valence band into heavy-hole and light-hole ones. The present results are closer to the reported data [39] from cyclotron-resonance measurements indicating that the optical reflectance analysis is also reliable to characterize the hole effective mass. For Raman scattering measurement, the electron or hole effective mass is required as a priori knowledge in order to obtain the free carrier concentration [22]. In the present work, we estimated the hole effective mass with about 3% uncertainty using the fitted plasma frequency, based on reliable carrier concentrations from Hall-effect measurements [24,32].

3.4 LO phonon plasmon coupled modes

To investigate in detail the behavior of the LPP coupled modes in *p*-type GaSb:Zn epilayers, the real and imaginary parts of the complex coupled mode frequency $\omega = \mathrm{Re}(\omega) + i\mathrm{Im}(\omega)$ should be determined [40]. This assumes that the electric field E has an $e^{i\omega t}$ time dependence. $\mathrm{Re}(\omega)$ and $\mathrm{Im}(\omega)$ are the mode frequencies modified by the free carrier damping and the damping degree of the coupled modes, respectively [21,40]. The LPP coupled modes are obtained using equation (5) while $\varepsilon(\omega)$ is equal to zero [40]:

$$\varepsilon_\infty + \frac{S\omega_{TO}^2}{\omega_{TO}^2 - \omega^2 - i\omega\Gamma} - \frac{\varepsilon_\infty \omega_p^2}{\omega^2 + i\omega\gamma} = 0. \quad (8)$$

Moreover, we consider the relationship $\omega_{LO}^2 = (S/\varepsilon_\infty + 1)\omega_{TO}^2$ and the solutions in the complex ω-plane are the coupled modes for the real part $\mathrm{Re}(\omega)$

$$[\mathrm{Re}(\omega_{LPP})]^2 = \frac{(\omega_p^2 + \omega_{LO}^2 + \gamma\Gamma)}{2} \pm \frac{\sqrt{(\omega_p^2 + \omega_{LO}^2 + \gamma\Gamma)^2 - 4\omega_p^2\omega_{TO}^2}}{2}, \quad (9)$$

and for the imaginary part $\mathrm{Im}(\omega)$

$$[\mathrm{Im}(\omega_{LPP})]^2 = \frac{\omega_{LO}^2\gamma + \omega_p^2\Gamma}{\gamma + \Gamma}. \quad (10)$$

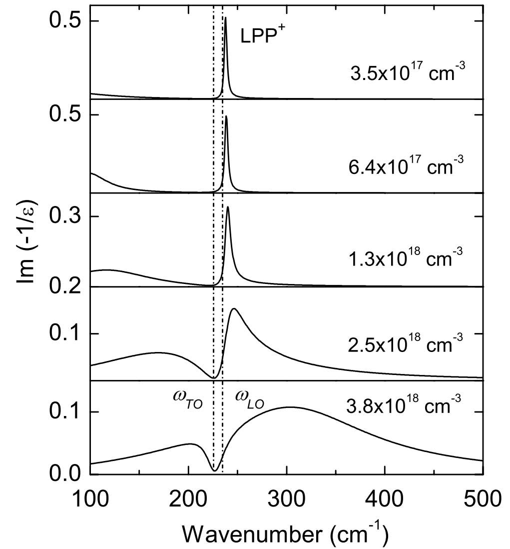

Fig. 5. The spectral density function $\mathrm{Im}(-1/\varepsilon)$ of the GaSb:Zn epitaxial films with different hole concentrations. Note that the vertical scale is different owing to the broadening from the LPP$^+$ mode.

From the above equations, $\mathrm{Re}(\omega_{LPP})$ and $\mathrm{Im}(\omega_{LPP})$ show a relatively complicated dependence on the plasma frequency and on the carrier damping constant. With increasing plasma frequency (normally the damping also increases), the coupling interaction and the distortion from the LO phonon increase. If the free carrier damping can be neglected (i.e., $\gamma = 0$), $\mathrm{Re}(\omega)$ becomes the well-known undamped LPP coupled modes:

$$[\mathrm{Re}(\omega_\pm)]^2 = \frac{(\omega_p^2 + \omega_{LO}^2) \pm \sqrt{(\omega_p^2 + \omega_{LO}^2)^2 - 4\omega_p^2\omega_{TO}^2}}{2}. \quad (11)$$

and $\mathrm{Im}(\omega)$ has $[\mathrm{Im}(\omega_\pm)]^2 = \omega_p^2$. In that case the LPP coupling interaction decreases and the real part of the complex-frequency only depends on the plasma frequency. The imaginary part of the complex-frequency is then the plasma frequency, indicating that the distortion disappears.

Figure 5 shows the spectral density function $\mathrm{Im}(-1/\varepsilon)$ of GaSb:Zn epitaxial films. The LO phonon becomes weaker and disappears owing to the coupling with the hole plasmon. Although there are two coupled modes from the above theoretical calculations (see Fig. 6), the lower branches of the LPP modes are not observed in the present work. This can be due to a higher damping constant and higher hole effective mass compared with *n*-type semiconductors [24]. The upper LPP$^+$ frequencies increase with the hole concentration and show a transition from phonon-like to plasmon-like behavior [9,21]. From Figure 5, we are also aware of another asymmetric peak below the TO-phonon frequency for the GaSb:Zn films with the three highest hole concentrations. However, compared with the LPP$^+$ modes the peaks are so broad and weak that they are strikingly different from the LPP$^-$ modes like those in *n*-type semiconductors, in which the damping constant is

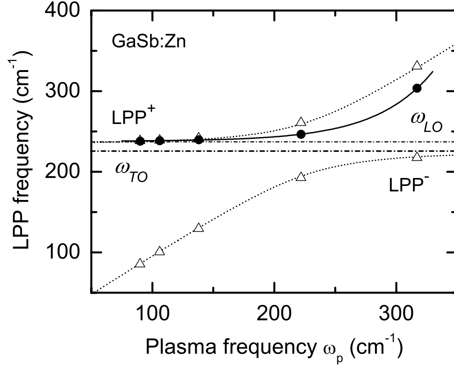

Fig. 6. The variations of the LPP^+ coupled mode (filled dots) with the plasma frequency from the spectral density function in Figure 5. The data (triangles) are from the solutions of Eq. (9) with the parameter values in Table 1. The dotted lines are the theoretical coupled modes using equation (11) without the free hole damping. Note that the data below the ω_{TO} frequency are only from theoretical calculations.

smaller [15]. Yuasa et al. concluded that the two branches of the LPP modes appear even for a *p*-type GaAs film with a hole concentration of 3.0×10^{18} cm^{-3} [41]. On the other hand, Fukasawa et al. argued that only LPP^- mode is observed and shifted to higher frequency in heavily doped *p*-type GaAs films, in which the hole concentration reaches up to 2.9×10^{19} cm^{-3} [42]. Note that the above results were from Raman scattering experiments, which have the difficulty of combining the complex Raman profile from the bulk material with the profile produced by the unscreened LO phonon in a surface depletion layer [42]. However, infrared reflectance spectra avoid the above disadvantages because the incident light can penetrate the GaSb:Zn films to the substrates, detecting the total contribution from the epilayers. In addition, the plasma frequency obtained from the FIR measurement usually depends on the experimental wavelength limit [30]. The optical measurements should extend to longer wavelengths (i.e., plasma frequency edges) for films with lower carrier concentration in order to distinguish the ambiguous behavior. It is for this reason that the asymmetric peaks below the TO-phonon frequency are not assigned to the LPP^- modes here.

The upper LPP^+ modes become broader with increasing hole concentration indicating that the coupling becomes stronger. The broadening of the LPP^+ mode is due to the higher damping constant, higher hole effective mass, and lower hole mobility compared with *n*-type materials [20]. The LPP coupled modes for GaSb:Zn films of different concentrations obtained from the maximum in $\mathrm{Im}(-1/\varepsilon)$, together with the solutions of $\mathrm{Re}(\omega)$, and the theoretical coupled modes without damping (setting the average value $\Gamma = 2.0$ cm^{-1}) are shown in Figure 6. It must be emphasized that the results below the TO-phonon frequency are only from calculations based on the previous analysis. One clearly sees that the results on the LPP^+ mode from the three methods are similar for hole concentrations below 1.0×10^{18} cm^{-3}. The data from the solutions of $Re(\omega)$ and the calculated coupled modes without damping agree well. This may be due to a smaller value of Γ and γ product compared with the squared values of the plasma frequency and LO-phonon frequency. However, with increasing hole concentration the LPP^+ coupled frequencies deviate from the experimental data. This indicates that the effect from the free hole damping increases and should be considered. Fukasawa et al. estimated the effects from different damping constants for *p*-type GaAs and found that the coupling remarkably increases with $\gamma \geq 450$ cm^{-1} [21,40,42]. For *p*-type GaSb:Zn films, a strong coupling is observed for a hole concentration of 2.5×10^{18} cm^{-3} with $\gamma = 193.6$ cm^{-1} owing to overdamping effects. It can be ascribed to the effects from a lower LO-phonon frequency (236 cm^{-1}) for the GaSb films. Compared with GaAs material, the LO- and TO-phonon frequencies of GaSb semiconductor are lower, which means that the coupling interaction can occur when the plasma frequency and damping are not high. This agrees well with the present FIR experimental observations for GaSb:Zn epilayers.

4 Conclusions

Reflectance spectra from *p*-type GaSb:Zn epitaxial films with different hole concentrations, grown by metalorganic vapor-phase epitaxy, have been measured in the frequency region of 100–1000 cm^{-1}. The Hall-mobility values are slightly larger than those obtained from infrared measurements. A detailed theoretical explanation in the Drude approximation has been presented. The LPP^+ frequency increases with hole concentration and shows a transition from phonon-like to plasmon-like behavior. Good agreement between the maximum of $\mathrm{Im}(-1/\varepsilon)$, the solution of $\mathrm{Re}(\omega)$, and the calculated coupled modes without free hole damping for the upper LPP^+ modes is achieved at low hole concentrations. This confirms the possibility to derive LPP coupled modes from infrared reflectance spectra of *p*-type GaSb:Zn films.

The work was supported in part by the U.S. NSF under grant No. ECS-0140434. The authors would like to acknowledge S.G. Matsik, G. Ariyawansa and A. Weerasekara for many fruitful discussions and technical support. M. Zhu acknowledges support from the 8th Participation in Research Program (PRP) project No. T0720811 of Shanghai Jiao Tong University.

References

1. P.S. Dutta, H.L. Bhat, V. Kumar, J. Appl. Phys. **81**, 5821 (1997)
2. M. Hass, B.W. Henvis, J. Phys. Chem. Solids **23**, 1099 (1962)
3. S. Zollner, M. Garriga, J. Humlek, S. Gopalan, M. Cardona, Phys. Rev. B **43**, 4349 (1991)
4. R. Pino, Y. Ko, P.S. Dutta, J. Appl. Phys. **96**, 1064 (2004)
5. V.S. Sundaram, P.E. Gruenbaum, J. Appl. Phys. **73**, 3787 (1993)

6. A.G.U. Perera, H.X. Yuan, M.H. Francombe, J. Appl. Phys. **77**, 915 (1995)
7. S.K. Ray, T.N. Adam, R.T. Troeger, J. Kolodzey, G. Looney, A. Rosen, J. Appl. Phys. **95**, 5301 (2004)
8. Z.G. Hu, A.G.U. Perera, Y. Paltiel, A. Raizman, A. Sher, J. Appl. Phys. **98**, 023511 (2005)
9. Z.G. Hu, M.B.M. Rinzan, S.G. Matsik, A.G.U. Perera, G. Von Winckel, A. Stintz, S. Krishna, J. Appl. Phys. **97**, 093529 (2005)
10. M.B.M. Rinzan, A.G.U. Perera, S.G. Matsik, H.C. Liu, Z.R. Wasilewski, M. Buchanan, Appl. Phys. Lett. **86**, 071112 (2005)
11. S. Adachi, J. Appl. Phys. **66**, 6030 (1989)
12. P.P. Paskov, J. Appl. Phys. **81**, 1890 (1997)
13. R. Ferrinia, M. Patrini, S. Franchi, J. Appl. Phys. **84**, 4517 (1998)
14. D.F. Edwards, R.H. White, *Handbook of Optical Constants of Solids II*, edited by E.D. Palik (Academic, New York, 1991)
15. G. Irmer, M. Wenzel, J. Monecke, Phys. Rev. B **56**, 9524 (1997)
16. H.R. Chandrasekhar, A.K. Ramdas, Phys. Rev. B **21**, 1511 (1980)
17. M. Chafai, A. Jaouhari, A. Torres, R. Antón, E. MartÍn, J. Jiménez, W.C. Mitchel, J. Appl. Phys. **90**, 5211 (2001)
18. T. Kaneto, K.W. Kim, M.A. Littlejohn, J. Appl. Phys. **72**, 4139 (1992)
19. K. Wan, J.F. Young, Phys. Rev. B **41**, 10772 (1990)
20. M. Seon, M. Holtz, W.M. Duncan, T.S. Kim, J. Appl. Phys. **85**, 7224 (1999)
21. R. Fukasawa, K. Sakai, S. Perkowitz, Jpn J. Appl. Phys. **36**, 5543 (1997)
22. L. Artús, R. Cuscó, J. Ibáñez, N. Blanco, G. González-DÍaz, Phys. Rev. B **60**, 5456 (1999)
23. J.S. Thakur, D. Haddad, V.M. Naik, R. Naik, G.W. Auner, H. Lu, W.J. Schaff, Phys. Rev. B **71**, 115203 (2005)
24. W. Songprakob, R. Zallen, W.K. Liu, K.L. Bacher, Phys. Rev. B **62**, 4501 (2000)
25. O.S. Heaven, *Optical Properties of Thin Solid Films* (Dover, NewYork, 1991)
26. R. Cuscó, J. Ibáñez, L. Artús, Phys. Rev. B **57**, 12197 (1998)
27. H. Lee, M.V. Klein, J. Appl. Phys. **81**, 1899 (1997)
28. P.D. Wang, M.A. Foad, C.M. Sotomayor-Torres, S. Thoms, M. Watt, P. Cheung, C.D.W. Wilkinson, S.P. Beaumont, J. Appl. Phys. **71**, 3754 (1992)
29. W.K. Metzger, M.W. Wanlass, L.M. Gedvilas, J.C. Verley, J.J. Carapella, R.K. Ahrenkiel, J. Appl. Phys. **92**, 3524 (2002)
30. T.E. Tiwald, J.A. Woollam, S. Zollner, J. Christiansen, R.B. Gregory, T. Wetteroth, S.R. Wilson, A.R. Powell, Phys. Rev. B **60**, 11464 (1999)
31. M. van Exter, D. Grischkowsky, Phys. Rev. B **41**, 12140 (1990)
32. K.C. Agarwal, B. Daniel, M. Grün, P. Feinäugle, C. Klingshirm, M. Hetterich, Appl. Phys. Lett. **86**, 181907 (2005)
33. W.G. Spitzer, H.Y. Fan, Phys. Rev. **106**, 882 (1957)
34. S.C. Shen, *Optical Spectrum and Properties of Semiconductors* (Science Publisher, Beijing, 2002)
35. P.Y. Yu, M. Cardona, *Fundamentals of Semiconductors* (Springer, Berlin, 1996)
36. A. Chandola, R. Pino, P.S. Dutta, Semicond. Sci. Technol. **20**, 886 (2005)
37. B.W. Kim, A. Majerfeld, J. Appl. Phys. **79**, 1939 (1996)
38. H.A. Lyden, Phys. Rev. **134**, A1106 (1964)
39. M.W. Heller, R.G. Hamerly, J. Appl. Phys. **57**, 4626 (1985)
40. R. Fukasawa, S. Perkowitz, Jpn. J. Appl. Phys. **35**, 132 (1996)
41. T. Yuasa, M. Ishii, Phys. Rev. B **35**, 3962 (1987)
42. R. Fukasawa, S. Perkowitz, Phys. Rev. B **50**, 14119 (1994)